ELSEVIER

Contents lists available at ScienceDirect

Optics Communications

journal homepage: www.elsevier.com/locate/optcom



Power scaling strategy for resonant second-harmonic generation in the visible regime

Manuel A. Medina * Sahar Alidousti, Callum McEwan, W. Andrew Clarkson

Optoelectronics Research Centre, University of Southampton, Southampton, SO17 1BJ, UK

ARTICLE INFO

Dataset link: https://doi.org/10.5258/SOTON/

Keywords:
Second harmonic generation
LBO
Multi-axial generation
SRS

ABSTRACT

In this paper, we describe external resonant second harmonic generation (SHG) of a multi-axial mode near-infrared (near-IR) source for scaling power in the visible (green) spectral band. By distributing the power across multiple frequencies, we significantly increased the output power obtainable from an ytterbium-doped fibre amplifier before reaching the onset of Stimulated Brillouin Scattering (SBS). Using a near-IR laser with ~9 longitudinal modes and an LBO crystal in a bow-tie cavity configuration, up to 15 W at a wavelength of 532 nm was achieved, with a conversion efficiency of 65% with respect to incident power. We discuss strategies for further up-scaling of output power, including increasing the number of axial modes and optimizing the amplifier configuration. Additionally, we highlight the advantages of our approach compared to previously reported high-power SHG systems, demonstrating its potential for future power scaling.

1. Introduction

Laser processing is increasingly being used for a wide range of materials, spanning from polymers to metals, requiring high power and high beam quality. Near-IR fibre lasers emitting around 1 μ m are particularly suited for different laser processing techniques, such as welding, drilling, and cutting. However, non-ferrous materials such as copper, gold, and silver are highly reflective at this wavelength [1]. In particular, the rising demand for electric vehicles and renewable energy sources has further increased the need for efficient, reliable laser processing of copper as a key material due to its high electrical conductivity. A laser emitting in the visible regime is better suited for this purpose owing to stronger absorption, as shown in Fig. 1.

An effective green laser for industrial applications should have high output power, good efficiency, and excellent beam quality. While the advantages of green lasers for copper welding and other industrial applications have been well established, only a few commercial and experimental systems have reached the high output powers needed for widespread adoption. Despite these advancements, many existing green laser systems face trade-offs between power, efficiency, and beam quality. In 2020, TRUMPF Laser GmbH produced a maximum power of 2 kW in the green wavelength via an intra-cavity frequency-doubled thin disk laser [2]. However, the output beam exhibited a high beam parametric product (BPP) of 6 mm·mrad (corresponding to an $M^2 \sim 36.6$) due to thermal effects of the disk laser. In the same year, Coherent reported a 1 kW laser beam emitted at 532 nm through single-pass (SP)

SHG in a 55 mm long LBO crystal with an optical conversion efficiency of 54 % [3]. Other notable demonstrations of high-power SP SHG in the green regime include 321 W with a beam quality of 1.07 and conversion efficiency of 40.9% [4], and 350 W with single-mode beam quality and 35 % conversion efficiency [5].

Traditionally, high-power green laser beams are generated through either SP SHG or external resonant SHG of near-IR sources. The first approach offers a simpler experimental setup, but the resulting conversion efficiencies in the non-linear crystal are relatively low (typically less than 40 %). To reach higher efficiency, the near-IR source should be in the multi-kW regime [6]. As a second main approach, resonant-enhanced SHG has proven to deliver conversion efficiencies of up to 90 % even at a few Watts [7,8]. As a drawback, this method requires a single-frequency narrow-linewidth source as a near-IR input, which poses significant challenges for power scaling. Despite the availability of high-power 1 µm fibre lasers, maintaining narrow-linewidth operation is challenging due to the onset of SBS in the amplifiers [9]. Several approaches have been investigated in the past to mitigate the effects of SBS. Most notably, these have included using large core fibres, introducing a thermal or stress distribution along the fibre length [10,11], and special designs of the active fibres [12,13]. Although effective, depending on the application, some of these methods can be difficult to implement. The most effective way to mitigate the SBS remains active broadening of the spectrum through phase modulation. However, due to the narrow resonance acceptance

E-mail address: m.a.medina@soton.ac.uk (M.A. Medina).

Corresponding author.

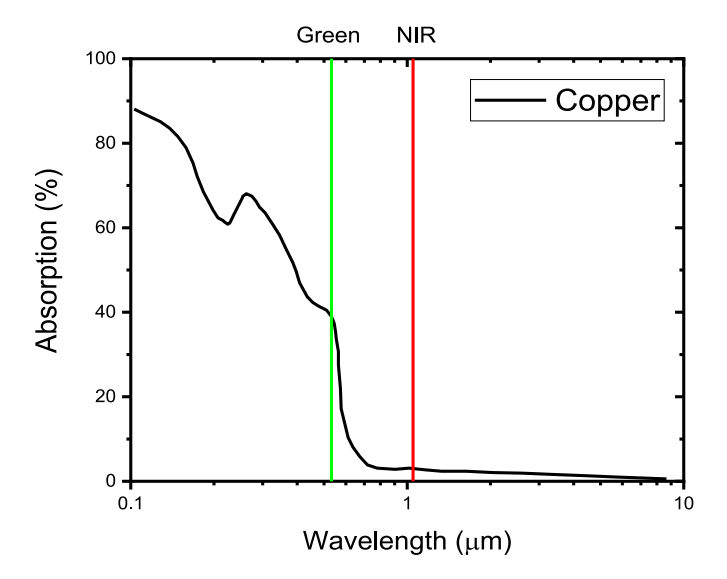


Fig. 1. Absorption of copper as a function of wavelength. *Source:* Image taken from [1].

bandwidth, this method cannot be exploited for efficient external resonant SHG. This has hampered the power scaling of such schemes, with the highest powers from external resonant SHG typically in the tens of Watts regime [14–17]. Even when considering solid-state bulk laser as seed sources, only a few reports exceeding hundreds of Watts have been made using external resonant SHG [18,19]. Thus, a method that retains the high efficiency of resonant SHG while allowing for power scaling beyond narrow-linewidth SBS limitations remains an open challenge.

In this article, we propose an external resonant SHG using a multiaxial mode source, offering a novel solution to the SBS limitation. A near-IR laser emitting ~ 8-10 axial modes is amplified and then used for efficient injection into a resonant SHG cavity. The linewidth of each individual axial mode is less than 10 kHz. Unlike conventional resonant SHG approaches that require single-frequency inputs, our method exploits the simultaneous resonance of multiple longitudinal modes, thereby enhancing power scalability of external resonant SHG. By distributing power across multiple axial modes, we mitigate SBS constraints, enabling higher amplifier output power before reaching the SBS threshold. This allows for significantly higher power scaling while maintaining the high conversion efficiency of resonant SHG, effectively overcoming the limitations faced by single-frequency sources. While our approach enables higher power scaling in resonant SHG, it introduces additional challenges, such as the need for precise impedance matching across multiple modes. Moreover, maintaining cavity resonance for all axial modes simultaneously requires high mechanical and thermal stability. We discuss the feasibility of this technique theoretically, and we present preliminary experimental results. Prospects for further development of this scheme, with a particular focus into power scaling, are also considered.

2. Theory

2.1. SBS suppression

SBS remains a fundamental barrier to achieve high output power in fibre lasers, particularly in narrow-linewidth systems for SHG aiming at the green spectral band. As the beam power in the fibre increases, SBS leads to a backward-propagating Stokes wave that limits power scaling. Therefore, effective strategies to mitigate SBS are essential to achieve high power. The threshold of the SBS can be estimated from [9]:

$$P^{th} \sim \frac{21 \cdot A_{eff}}{g_B(\Delta v) L_{eff}} \tag{1}$$

where A_{eff} is the effective area of the fibre core and $g_B(\Delta v)$ is the Brillouin gain coefficient, which is dependent on the signal linewidth. It is characterized by a Lorentzian spectral dependence and its expression can be found in [20]. L_{eff} is the effective interaction length. In the case of passive fibres, it is expressed as $(1-e^{-\alpha L})/\alpha$, with α being the fibre propagation loss and L the physical length. However, when considering high-power fibre amplifiers, the presence of gain in the active medium causes the signal to experiences a substantially different distribution along the fibre. Consequently, only a small portion of the length experiences high-power, leading to a much shorter effective length, thus higher SBS thresholds. Eq. (1) holds true when the linewidth of the laser is much lower than the Brillouin gain bandwidth, which in silica fibres is typically between 10 and 100 MHz depending on the fibre [20,21]. If we consider a narrow linewidth signal of ~ 10 kHz, a typical value for g_B in silica fibres is $5 \cdot 10^{-11}$ W/m. To evaluate the impact of SBS, let us consider a single mode (SM) fibre with 10 µm core diameter and a length of 10 m. Based on Eq. (1), the calculated Pth would be around 3 W. In reality, due to the shorter interaction length, this value is usually somewhat higher for active fibres. Several approaches have been investigated in the past to mitigate the effects of SBS and increase Pth. However, most techniques are incompatible with the requirements for external resonant SHG. Another way to counteract the onset of SBS while maintaining narrow-linewidth operation is needed.

Our proposed method would be to use a multi-axial source as signal beam. Emitted by the same gain medium, the spacing between the different longitudinal modes is determined by the free spectral range (FSR) of the cavity. This is determined by its geometrical length: FSR = c/L, where L is the optical round-trip length of the resonator. At first, let us consider the case where the total power P^{tot} is divided equally between N different modes, each with power $P_i = P^{tot}/N$. If this frequency difference between two adjacent axial modes is greater than the Brillouin gain bandwidth Δv_B , each single mode will experience a different Brillouin gain. Consequently, the SBS threshold will be reached when every single longitudinal mode reaches Pth. Hence, the effective threshold power of the system will increase by a factor of N: $P^{th}_{eff} = P^{th} \cdot N$. In a real system however, the power is not uniformly distributed, leading to deviations from this ideal scenario. The improvement factor will therefore be lower than N:

$$P_{eff}^{th} = \frac{P^{th} \cdot P^{tot}}{P_i^{max}},\tag{2}$$

where P_i^{max} is the power of the ith mode with the strongest power content. Even in this case though, by distributing the power along multiple longitudinal modes, we effectively decrease the energy available for SBS to build up in any single mode. An additional effect that must be consider is the dynamic of the system. Due to mode competition and mode hopping, the power distribution among the modes is not only unequal, but constantly fluctuates. This will lead to a time-averaged SBS threshold, which will depend on gain medium and resonator stability. Eq. (2) is therefore only an estimate and the real value of the SBS threshold could differ experimentally.

Compared to conventional SBS suppression methods such as phase modulation and temperature gradient techniques, multi-axial mode operation provides a passive and efficient approach that does not introduce additional optical losses or distortions. While phase modulation can achieve SBS suppression factors comparable to multi-axial operation, it typically requires broadening the spectrum to linewidths incompatible with SHG resonant cavities. In contrast, multi-axial mode operation achieves suppression without increasing the spectral width of individual modes, preserving the phase-matching conditions necessary for high-efficiency SHG. The main limitation of such method lies on the condition that the frequency spacing between the different longitudinal modes must be greater than the Brillouin gain bandwidth, ensuring minimal overlap in Brillouin gain contributions. If the FSR is smaller than Δv_R , the modes partially share the same Brillouin gain, reducing the effective suppression factor. An appropriate FSR therefore must be chosen when designing the multi-axial seed source.

Fig. 2. Schematic of the experimental setup. The 1064 nm beam image before coupling into the resonant cavity is shown. ISO = optical isolator. YDFA = Yb-doped fibre amplifier. HWP = half-wave plate. PD = photodetector. HR = high reflective mirrors. F1 = 4.6 mm. F2 = 250 mm.

2.2. Impedance-matched SHG

When considering an external enhancement cavity, it is possible to select the transmission coefficients of the input and output couplers to couple the input power without any rejected light from the input coupler (IC). Such condition is called impedance matching and it is achieved when the transmission T of the IC is equal to the sum of all the losses L in the resonator, T=L [22]. The loss term includes all other mirrors transmissions, the absorption and scattering of all the other elements within the resonator and, in the case of SHG, the nonlinear conversion in the non-linear crystal. When such condition is met, the circulating intra-cavity power is maximized: $P_{cav} = P_{in}/T$, with P_{in} the near-IR input power. In the case of multiple longitudinal operation, a particular attention must be placed on the optimization of the IC as the power increases. When considering every single longitudinal mode i, the individual SHG efficiency is given by the power dependent term [23]:

$$\eta_{SHG}^{i} = \tanh^{2} \sqrt{\gamma_{SHG}^{i} P_{cav}^{i}}.$$
 (3)

The factor γ^i_{SHG} depends on the non-linear crystal properties and focusing conditions [6]:

$$\gamma_{SHG}^{i} = \frac{2\omega_{i}^{3} d_{eff}^{2}}{\pi \epsilon_{0} c^{4} n^{2}} \cdot l \cdot h(\Delta k, \rho, \xi), \tag{4}$$

where ω_i is the ith near-IR frequency, d_{eff} is the effective non-linear coefficient, ϵ_0 is the vacuum permittivity, c is the speed of light, n is the refractive index, l is the optical crystal length, and $h(\Delta k, \rho, \eta)$ is the Boyd–Kleinman function, depending on the phase mismatch Δk , the walk-off angle ρ and the confocal parameter ξ .

However, unlike single-frequency SHG, the interaction of different longitudinal modes generates additional frequency components due to sum-frequency generation (SFG). The associated conversion efficiency presents a similar expression to Eq. (3), with a cross-coupling term given by:

$$\gamma_{SFG}^{ij} = \frac{2\omega_i \omega_j \omega_{i+j} d_{eff}^2}{\pi \epsilon_0 c^4 n^2} \cdot l \cdot h(\Delta k, \rho, \xi), \tag{5}$$

 ω_{i+j} being the frequency of the generated sum-frequency term. Thus, each individual frequency has a total associated loss:

$$L_i = L_i^{lin} + L_i^{SHG} + \sum_{i \neq i}^N L_{ij}^{SFG}, \tag{6}$$

where L_i^{lin} represents the linear cavity losses (mirror transmission, scattering, absorption) and the sum for the SFG terms is over all the possible interaction with the other frequencies. Previous studies on single-pass multi-axial mode SHG have proven, both theoretically and experimentally, that due to sum-frequency mixing, the total non-linear conversion losses can be up to twice as high, depending on

the number of longitudinal modes considered [24–26]. In principle, impedance matching should be optimized for each axial mode since they do not all share the same power content. This would require an IC with a different transmission $T_i = L_i$ for each individual mode. However, in practical implementations, this condition is difficult to achieve. The total bandwidth of the emitted axial modes typically lies within a few GHz, making it complex to design a mirror with mode-dependent transmission. Additionally, due to mode hopping, the power distribution between the axial modes is not constant over time. As a result, a time-averaged loss L_i must be considered for each longitudinal mode, depending on the seed resonator stability. The IC transmission must therefore be optimized experimentally to balance efficiency across all modes.

3. Experimental setup and results

3.1. Experimental setup

To validate our theoretical predictions, we implemented an experimental setup designed to assess the feasibility of multi-axial mode SHG. The scheme of the experimental setup used is presented in Fig. 2. A laser with a linear geometry having a multi-axial mode output was used as the seed laser. The physical length of the cavity was 250 mm and the gain medium was a 5 mm long $Nd: YVO_4$ crystal. It was pumped by a continuous-wave (CW), 4 W laser diode emitting at 808 nm (Lumics GmbH). The gain medium was placed close to the IC to enhance the number of modes emitted due to spatial hole burning [27]. The fundamental waist at the laser medium was $\sim 300~\mu m$. The 1064 nm output beam was linearly polarized and with a maximum output power of 600 mW. The output spectrum was investigated through the use of a commercial scanning Fabry-Perot interferometer (Thorlabs, Inc.), with a FSR of 10 GHz. The result is presented in Fig. 3. Although the number of emitted axial mode frequencies varied slightly during operation due to mode hopping, it stayed stably above 8, with an average of 9. The beam was then amplified in an Yb-doped fibre amplifier. The fibre was a polarization maintaining, single mode fibre with a core diameter of 10 µm, a cladding diameter of 125 µm and a numerical aperture (NA) of 0.46. Its length was 10 m. A small amount of distortion of the beam shape was observed at the output, which was attributed to phase aberration due to an imperfect end-cap fused to the output end of the fibre, as can be seen in Fig. 2. This beam was then mode-matched to the resonant cavity using two lenses, F1 = 4.6 mm and F2 = 250 mm. The waist size in the long arm of the resonator was $\sim 250 \ \mu m$. The fundamental mode size in the non-linear crystal was $\omega = 52 \mu m$. A half-wave plate and an isolator were used to achieve isolation from the residual reflection from the AR-coated LBO crystal. An additional half-wave plate was used to allow fine adjustment of the polarization direction for optimum SHG. The SHG resonant cavity had a bow-tie configuration, using two flat mirrors and two concave mirrors with a

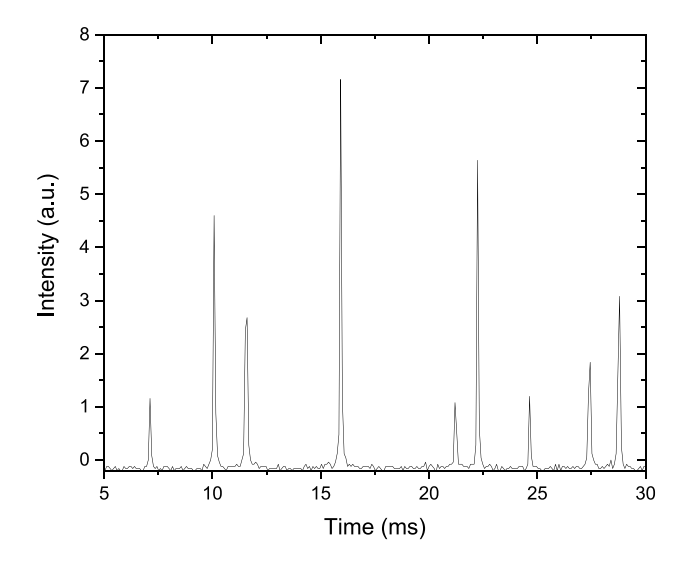


Fig. 3. Multi-axial mode spectrum of the $Nd: YVO_4$ laser.

radius of curvature ROC=100 mm. The angle of incidence was 6° and the total round-trip cavity length was ~ 500 mm to match the round-trip length of the near-IR seed source.

From Eq. (3), the non-linear conversion losses of the cavity grow as the power in the resonator increases. Consequently, depending on the power level, an input mirror with a different transmission T must be used to achieve the optimum enhancement condition. In our set-up, the best coupling into the cavity was achieved using an input mirror M1 with a transmission T = 4 %. All the other mirrors in the resonant cavity were highly reflective at 1064 nm. In addition, M4 was highly transmittive at 532 nm. M2 was attached to a piezoelectric translation stage to enable length matching with the seed laser cavity. Active length stabilization was not implemented and the cavity was scanned through resonance with the piezo. For SHG, an LBO crystal with dimensions of 3 x 3 x 15 mm³ was used. The crystal was placed in an oven to stabilize its temperature and the phase-matching (PM) was obtained through angle tuning (critical PM). The phase-matching acceptance bandwidth of the LBO, dependent on temperature, is typically as broad as 2-3 nm, corresponding to > 500 GHz [28]. Since all our axial-modes lie within few GHz, all our longitudinal modes lie well within the acceptance bandwidth and the deviation in efficiency is negligible.

3.2. Experimental results

The onset of the SBS was monitored by checking the backpropagating power from the amplifier as a function of the output power. The result is presented in Fig. 4(a). Although in literature there are various definitions for the SBS threshold, the most common is by comparing the back-propagating power as some fraction of the signal power: $P^{th} = \mu P_S$. Due to the exponential behaviour of the power close to threshold, the exact value of μ is not crucial, with values ranging from 1 to 0.001 in the literature [13]. In our setup, the reverse direction port of the isolator was monitored to give a measure of the back-propagating power. As this does not provide access to the full backward propagating power we chose a conservative (safe) value of $\mu = 1.5 \cdot 10^{-4}$. According to this definition, we can therefore observe the typical steep increase related to SBS of the backwards power at around 35 W of output power in Fig. 4(a), indicating the onset of SBS. The amplifier was not operated beyond this point to avoid any damage. In order to evaluate the improvement due to the multi-axial-mode approach, the same amplifier was used with a narrow-linewidth (~ 10 kHz) single-frequency 1064 nm laser. Its results are presented in Fig. 4(b). In the case of single-frequency operation, the maximum power

obtained before reaching SBS threshold was 6 W. The improvement in the Pth given by the multi-frequency source is lower than the predicted theoretical value ($P^{th} \cdot N$, with N = 9). The discrepancy can be explained by the non-uniform power distribution across the longitudinal mode spectrum presented in Fig. 3. In general, different frequencies do not have the same power and, in particular, the highest longitudinal mode contains $\sim 25 \%$ of the total power. Consequently, this particular axial mode will reach the SBS threshold (6 W) first. Based on Eq. (2), the maximum power obtainable before reaching the SBS threshold should be around 24 W, lower than our experimental value. However, an additional effect to be taken into account is the continuous mode hopping and the resulting power exchange between the different axial modes. Hence, while Fig. 3 can be used to extrapolate some information about the mode structure of the different modes, the specific power distribution constantly changes, although the number of emitted modes stays relatively stable. This effect operates on a time scale (ms) much shorter than the time response of the thermal power meters used in the experiment. Therefore, the power values measured in Fig. 4 represent only an average power distribution, not necessarily the one measured in Fig. 3. Stabilization of the seed cavity would be needed to avoid such discrepancy and exactly link the power distribution between the modes and Pth. Nevertheless, an improvement factor of 6 was obtained even in this non ideal configuration.

To achieve efficient impedance matching, the transmission of the input mirror has to match the total losses of the cavity, including the non-linear conversion. Since the SHG efficiency is power dependent, each axial mode will experience a different non-linear loss. Additionally, the losses due to the sum-frequency mixing (SFM) between the several modes have to be considered as well. Consequently, input mirrors with different transmission have been used. The best matching was found operating with a mirror of transmission T = 4% as M1. A maximum coupling efficiency of 85 % into the resonant cavity was obtained. This imperfect value was attributed to the beam distortion caused by the end-cap of the amplifier (see Fig. 2). Indeed, any non- TEM_{00} contribution of the beam would be rejected by the resonant cavity. The resonator was scanned through resonance with the use of a piezo translation stage. In order to have all the frequencies resonant at the same time, the cavity must be length-matched to the seed laser. This was accomplished by monitoring with a photo-detector (PD) the 1064 nm transmitted through M3. When the lengths of the two resonators are not equal multiple output peaks, corresponding to the different axial modes, are observed, as shown in Fig. 5(a). With a translational stage, the length of the resonator was tuned to collapse all the axial modes into a single peak, indicating length matching between the two resonators. This configuration is presented in Fig. 5(b). Although the seed laser presents intrinsic mechanical instabilities, they do not have an effect on the length matching procedure. Indeed, even in the case of mode hopping or power exchange between existing axial modes, the SHG cavity will still satisfy the resonant condition for the new emitted longitudinal modes. Consequently, the stability of the emitted peaks is only directly linked to the power stability of the seed laser.

The second harmonic power (including SFM power) as a function of coupled power is presented in Fig. 6. Due to the end-cap distortion, from the available near-IR power, a maximum of 24 W was coupled into the resonator (and consequently into the LBO). As a result, a maximum of 15 W of 532 nm was obtained, corresponding to a conversion efficiency of 65 %. Such conversion efficiency is comparable with previous reports [29], demonstrating the feasibility of a multifrequency approach. Since only the fundamental transverse mode could be supported in the resonator, the beam quality of the SHG beam was diffraction limited, although it presented an elliptical shape due to the astigmatic nature of the cavity, as presented on the inset in Fig. 6. Since the cavity was scanned through resonance, there was no significant thermal load on the non-linear crystal. Consequently, the beam image remained stable during operation. An active stabilization method of the

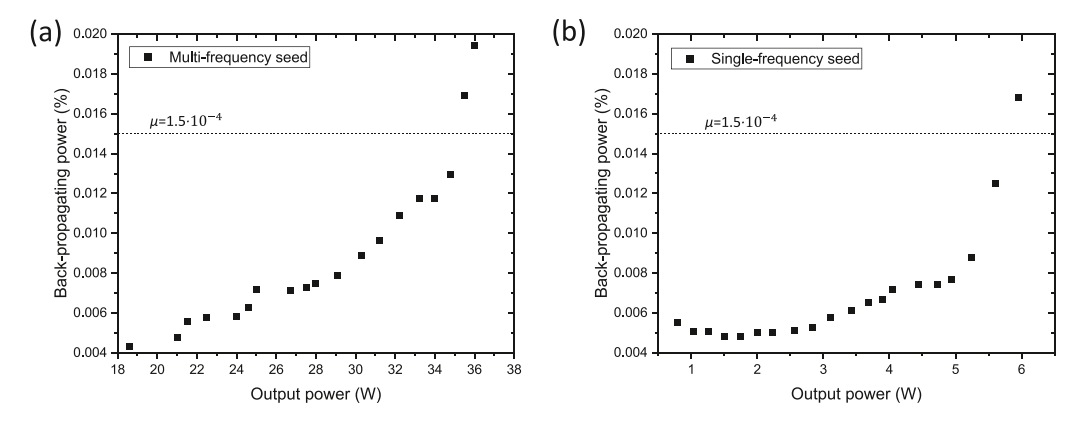


Fig. 4. Backward power as a function of the output power in the YDFA. (a) Multi-frequency seed laser. (b) Single frequency seed laser.

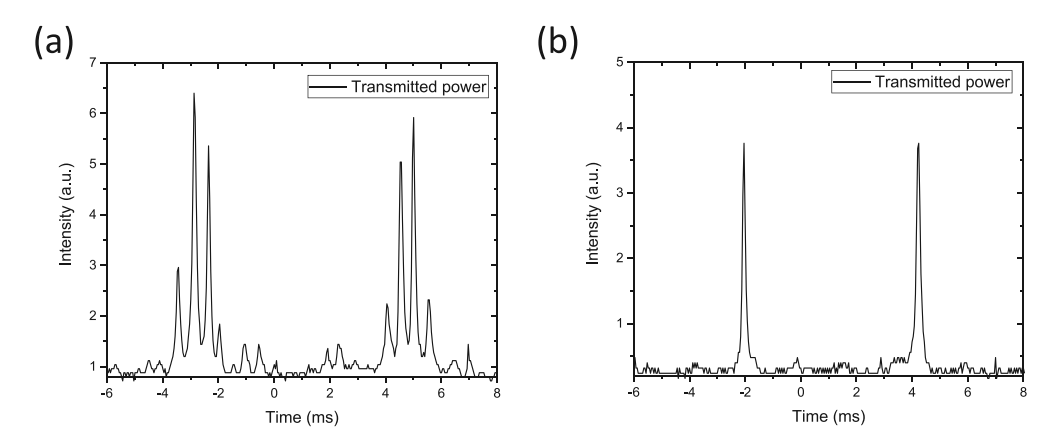


Fig. 5. (a) SHG cavity output peaks when length is not matched to the seed resonator. (b) SHG cavity output peaks when length is matched to the seed resonator.

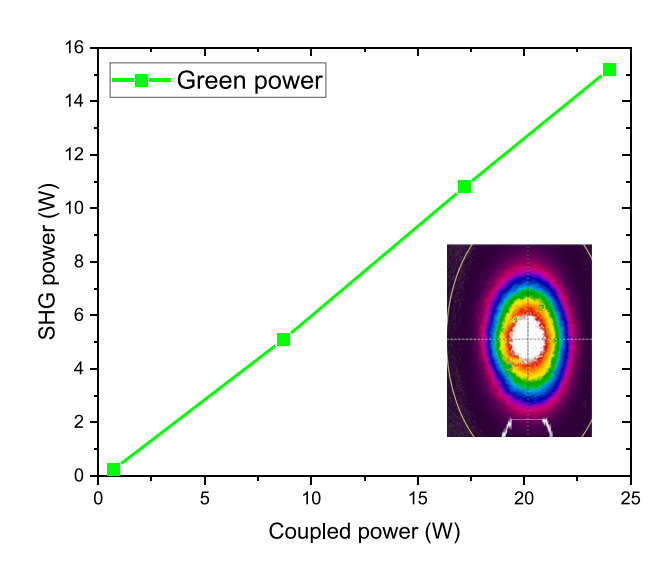


Fig. 6. SHG output power as a function of the input power. The output beam image is shown

resonator will have to be implemented to investigate on any thermal effects in the LBO and to carry out a power stability measurement. Linear polarization of the 532 nm beam was assured by the use of a Nd: YVO_4 as a gain material in the seed laser and the use of polarization maintaining fibre in the Yb-doped amplifier.

The results are currently limited by SBS in the fibre amplifier. Further scaling can be anticipated, as will be discussed in the next section.

4. Power scaling strategies

Based on the results obtained in our setup, we now explore methods to further scale power in our system. Currently, the main limitation of our experimental setup lies in the SBS limit in the Yb-doped amplifier. Hence, any strategy for further power scaling would necessarily have to address this issue. One way to further increase the SBS threshold would be to spread the seed power over an even larger number of axial modes. As long as they lie within the LBO phase-matching bandwidth and they are separated by at least the Brillouin gain bandwidth, the impact of SBS can be significantly reduced. If we consider the gain bandwidth of a Nd: YVO_4 crystal, it is approximately ~ 300 GHz. As the Brillouin gain bandwidth is typically $\lesssim 100$ MHz, theoretically, hundreds of longitudinal modes will satisfy such a requirement. In practice though, due to spatial hole burning, only a handful of axial modes will be emitted before saturation in the gain medium occurs [30,31]. Moreover, the implementation of longer cavities would lead to poorer mechanical stability. Therefore, other methods must also be considered. A particularly interesting and relatively easy way to increase the number of modes would be to implement a periodic phase modulation of the signal [29]. If the modulation frequency is chosen correctly and the frequency spacing is a multiple of the FSR of the SHG cavity, the resonance condition will still hold for all the generated frequencies.

Besides the use of a multi-axial-mode source laser, traditional methods for SBS mitigation can also be considered. The most straightforward way to overcome the SBS effect would be to use an additional Yb-doped amplifier with a larger core diameter, effectively increasing A_{eff} in Eq. (1). To quantify the improvement, we can consider a typical large mode area fibre commercially available, with a core diameter of 25 μ m. Since SHG cavity requires a single mode beam as input, we need to

consider the mode field diameter when evaluating A_{eff} . In addition to increasing the core diameter, a larger core allows us to shorten the length of the active fibre in the amplifier. We can then assume $L_{eff} \sim L = 5$ m. The improvement factor in SBS threshold can then be calculated as the ratio of Pth for the two fibres:

$$\frac{P_2^{th}}{P_1^{th}} = \frac{A_{eff,2} L_{eff,1}}{A_{eff,1} L_{eff,2}} \approx 7.6. \tag{7}$$

The maximum 1 μm output obtained in Section 2 was 35 W. The use of this new amplifier would then allows use to reach approximately 270 W

Further power scaling can be obtained by applying a temperature gradient along the active fibre of the amplifier. The root cause of SBS lies in the interaction between the optical signal and the acoustic waves in the fibre core. At any distance these acoustic waves have a Brillouin gain coefficient at frequency ν given by [10]:

$$g_B(\nu, T) = g_0 \frac{(\Delta \nu_B/2)^2}{(\nu - \nu_B(\Delta T))^2 + (\Delta \nu_B/2)^2} \tag{8}$$

where g_0 is the peak value of the Brillouin gain spectrum, Δv_R is the Brillouin gain bandwidth and $v_R(\Delta T)$ is the frequency downshift due to the temperature distribution ΔT , which includes both the external temperature modulation, and the temperature change in the fibre core caused by absorption of the pump beam and consequent heating due to the laser pumping cycle [32]. From Eq. (8), by applying a temperature distribution along the active fibre, different sections of the fibre will experience Brillouin gain at different frequencies, effectively disrupting the coherent build-up of the back-propagating signal [33]. If the frequency shift is greater than the Brillouin gain linewidth, the signal will effectively experience lower gain, leading to an increase in Pth. Predicting the impact of the temperature distribution on the SBS threshold is not immediately obvious. Precise calculations and simulations require the knowledge of the exact values of the different quantities involved in Eq. (8). These can vary according to the setup and type of fibre used. Hence, experimental measurement of them must be carried out before evaluating their effect on Pth. However, multiple dBs of improvement have been reported previously with relatively simple setups [10,32]. It seems therefore worthwhile pursuing such scheme for further power scaling the 1064 nm source.

Applying all these improvements will allow us to reach hundreds of Watts of near-IR for SHG. The implementation of a resonant cavity at such high power levels will require careful evaluation of the thermal effects in the LBO crystal. The thermal load and consequent thermal lensing will play a role in degrading the beam quality and stability of the output beam. Although thermal considerations are outside the scope of this paper, they will have to be considered in future work to achieve efficient high-power SHG.

5. Conclusions

We presented a high-power 532 nm laser through external resonant SHG using a multi-axial-mode as 1064 nm source. The near-IR laser, emitting 9 longitudinal modes, allowed us to significantly increase the SBS threshold in the fibre amplifier by a factor of 6. The maximum green power obtained was 15 W, corresponding to 65 % of conversion efficiency. This result demonstrates the feasibility of this approach. Strategies for future power scaling of the setup were discussed, paving the way to power scaling of external resonant SHG in the green spectral band for applications in areas such as advanced copper processing.

CRediT authorship contribution statement

Manuel A. Medina: Writing – review & editing, Writing – original draft, Investigation. Sahar Alidousti: Investigation. Callum McEwan: Conceptualization. W. Andrew Clarkson: Writing – review & editing, Conceptualization.

Funding

This work was supported by the Engineering and Physical Sciences Research Council, United Kingdom (EP/W028786/1).

Declaration of competing interest

The authors declare that they have no known competing financial interests or personal relationships that could have appeared to influence the work reported in this paper.

Data availability

All dataset used for this article are available at the following DOI address: https://doi.org/10.5258/SOTON/D3252.

References

- E. Punzel, F. Hugger, R. Dörringer, T.L. Dinkelbach, A. Bürger, Comparison of different system technologies for continuous-wave laser beam welding of copper, Proc. CIRP 94 (2020) 587–591, 11th CIRP Conference on Photonic Technologies [LANE 2020].
- [2] S. Pricking, E.-M. Dold, E. Kaiser, A. Killi, S. Bisch, S. Zaske, F. Baumann, R. Brockmann, 2 kW cw laser in the green wavelength regime for copper welding, in: Solid State Lasers XXIX: Technology and Devices, Vol. 11259, SPIE, International Society for Optics and Photonics, 2020.
- [3] P. Ahmadi, D. Creeden, D. Aschaffenburg, V. Mokan, M. Underwood, A. Caprara, Q.-Z. Shu, L. Spinelli, J. Minelly, I. Nikolov, Generating kW laser light at 532 nm via second harmonic generation of a high power Yb-doped fiber amplifier, in: Nonlinear Frequency Generation and Conversion: Materials and Devices XIX, 11264, SPIE, International Society for Optics and Photonics, 2020.
- [4] M. Su, Y. You, Z. Quan, H. Shen, Q. Li, W. Liu, Y. Qi, J. Zhou, 321 W high-efficiency continuous-wave green laser produced by single-pass frequency doubling of narrow-linewidth fiber laser, Appl. Opt. 60 (13) (2021) 3836–3841.
- [5] V. Gapontsev, A. Avdokhin, P. Kadwani, I. Samartsev, N. Platonov, R. Yagodkin, SM green fiber laser operating in CW and QCW regimes and producing over 550 W of average output power, in: Nonlinear Frequency Generation and Conversion: Materials, Devices, and Applications XIII, Vol. 8964, SPIE, International Society for Optics and Photonics, 2014.
- [6] S. Khripunov, S. Kobtsev, D. Radnatarov, Efficiency of different methods of extra-cavity second harmonic generation of continuous wave single-frequency radiation, Appl. Opt. 55 (3) (2016) 502–506.
- [7] S. Ast, R.M. Nia, A. Schönbeck, N. Lastzka, J. Steinlechner, T. Eberle, M. Mehmet, S. Steinlechner, R. Schnabel, High-efficiency frequency doubling of continuous-wave laser light, Opt. Lett. 36 (17) (2011) 3467–3469.
- [8] W. Yao, Q. Wang, L. Tian, R. Li, S. Shi, J. Wang, Y. Wang, Y. Zheng, Realizing high efficiency 532 nm laser by optimizing the mode- and impedance-matching, Laser Phys. Lett. 18 (1) (2020) 015001.
- [9] R.G. Smith, Optical power handling capacity of low loss optical fibers as determined by stimulated Raman and brillouin scattering, Appl. Opt. 11 (11) (1972) 2489–2494.
- [10] J. Hansryd, F. Dross, M. Westlund, P.A. Andrekson, S.N. Knudsen, Increase of the SBS threshold in a short highly nonlinear fiber by applying a temperature distribution, J. Lightwave Technol. 19 (11) (2001) 1691.
- [11] L. Zhang, S. Cui, C. Liu, J. Zhou, Y. Feng, 170 W, single-frequency, single-mode, linearly-polarized, Yb-doped all-fiber amplifier, Opt. Express 21 (5) (2013) 5456–5462
- [12] D. Engin, W. Lu, M. Akbulut, B. McIntosh, H. Verdun, S. Gupta, 1 kW cw Yb-fiber-amplifier with <0.5GHz linewidth and near-diffraction limited beam-quality for coherent combining application, in: J.W. Dawson (Ed.), Fiber Lasers VIII: Technology, Systems, and Applications, Vol. 7914, SPIE, International Society for Optics and Photonics, 2011, 791407.</p>
- [13] A. Kobyakov, S. Kumar, D.Q. Chowdhury, A.B. Ruffin, M. Sauer, S.R. Bickham, R. Mishra, Design concept for optical fibers with enhanced SBS threshold, Opt. Express 13 (14) (2005) 5338–5346.
- [14] S. Cui, L. Zhang, H. Jiang, W. Pan, X. Yang, G. Qin, Y. Feng, High efficiency frequency doubling with a passive enhancement cavity, Laser Phys. Lett. 16 (3) (2019) 035105.
- [15] P. Zeil, A. Zukauskas, S. Tjörnhammar, C. Canalias, V. Pasiskevicius, F. Laurell, High-power continuous-wave frequency-doubling in KTiOAsO₄, Opt. Express 21 (25) (2013) 30453–30459.
- [16] H.-Z. Chen, X.-P. Liu, X.-Q. Wang, Y.-P. Wu, Y.-X. Wang, X.-C. Yao, Y.-A. Chen, J.-W. Pan, 30 W, sub-kHz frequency-locked laser at 532 nm, Opt. Express 26 (26) (2018) 33756–33763.
- [17] R. Cieslak, W.A. Clarkson, Internal resonantly enhanced frequency doubling of continuous-wave fiber lasers, Opt. Lett. 36 (10) (2011) 1896–1898.

- [18] T. Meier, B. Willke, K. Danzmann, Continuous-wave single-frequency 532 nm laser source emitting 130 W into the fundamental transversal mode, Opt. Lett. 35 (22) (2010) 3742–3744.
- [19] A. Avdokhin, V. Gapontsev, Y. Grapov, 170W continuous-wave single-frequency single-mode green fiber laser, 2012, pp. XIX–XX.
- [20] M. Nikles, L. Thevenaz, P. Robert, Brillouin gain spectrum characterization in single-mode optical fibers, J. Lightwave Technol. 15 (10) (1997) 1842–1851.
- [21] A. Yeniay, J.-M. Delavaux, J. Toulouse, Spontaneous and stimulated brillouin scattering gain spectra in optical fibers, J. Lightwave Technol. 20 (8) (2002) 1425–1432
- [22] A. Ashkin, G. Boyd, J. Dziedzic, Resonant optical second harmonic generation and mixing, IEEE J. Quantum Electron. 2 (6) (1966) 109–124.
- [23] D. White, E. Dawes, J. Marburger, Theory of second-harmonic generation with high-conversion efficiency, IEEE J. Quantum Electron. 6 (12) (1970) 793–796.
- [24] J. Ducuing, N. Bloembergen, Statistical fluctuations in nonlinear optical processes, Phys. Rev. 133 (1964) A1493–A1502.
- [25] Y. Qu, S. Singh, Second-harmonic generation and photon bunching in multimode laser beams, Phys. Rev. A 47 (1993) 3259–3263.
- [26] W.-L. Zhou, Y. Mori, T. Sasaki, S. Nakai, Theoretical analysis of multimode pumped second-harmonic generation, Japan. J. Appl. Phys. 34 (10R) (1995) 5606.

- [27] B. Braun, K.J. Weingarten, F.X. Kartner, U. Keller, Continuous-wave mode-locked solid-state lasers with enhanced spatial hole burning, Appl. Phys. B 61 (1995) 429–437.
- [28] K.-H. Hong, C.-J. Lai, A. Siddiqui, F. Kärtner, 130-W picosecond green laser based on a frequency-doubled hybrid cryogenic Yb:YAG amplifier, Opt. Express 17 (2009) 16911–16919.
- [29] X. Zeng, S. Cui, X. Cheng, J. Zhou, W. Qi, Y. Feng, Resonant frequency doubling of phase-modulation-generated few-frequency fiber laser, Opt. Lett. 45 (17) (2020) 4944–4947.
- [30] Y.F. Chen, Y.J. Huang, P.Y. Chiang, Y.C. Lin, H.C. Liang, Controlling number of lasing modes for designing short-cavity self-mode-locked Nd-doped vanadate lasers, Appl. Phys. B 103 (2011) 841–846.
- [31] C. Serrat, C. Masoller, Modeling spatial effects in multi-longitudinal-mode semiconductor lasers, Phys. Rev. A 73 (2006) 043812.
- [32] Z. Lou, K. Han, X. Wang, H. Zhang, X. Xu, Increasing the SBS threshold by applying a flexible temperature modulation technique with temperature measurement of the fiber core, Opt. Express 28 (9) (2020) 13323–13335.
- [33] Y. Imai, N. Shimada, Dependence of stimulated Brillouin scattering on temperature distribution in polarization-maintaining fibers, IEEE Photonics Technol. Lett. 5 (11) (1993) 1335–1337.